Ultralow Doping in Organic Semiconductors: Evidence of Trap Filling

Selina Olthof,[1,*] Shafigh Mehraeen,[2] Swagat K. Mohapatra,[2] Stephen Barlow,[2] Veaceslav Coropceanu,[2] Jean-Luc Brédas,[2] Seth R. Marder,[2] and Antoine Kahn[1,†]

[1]*Department of Electrical Engineering, Princeton University, Princeton, New Jersey 08544, USA*

[2]*Center for Organic Photonics and Electronics and School of Chemistry and Biochemistry, Georgia Institute of Technology, Atlanta, Georgia 30332-0400, USA*

(Received 19 May 2012; published 26 October 2012)

Tail states in organic semiconductors have a significant influence on device performances by acting as traps in charge transport. We present a study of the controlled passivation of acceptor tail states in fullerene C_{60} by the addition of electrons introduced by molecular *n* doping. Using ultralow doping, we are able to successively fill the traps with charges and examine the changes in conductivity, activation energy, mobility, and Fermi-level position. Passivation of the traps leads to an increase of the electron mobility in C_{60} by more than 3 orders of magnitude, to reach 0.21 $cm^2/(V\,s)$.

DOI: 10.1103/PhysRevLett.109.176601 PACS numbers: 72.80.Le, 61.43.Bn, 79.60.Fr, 81.05.Fb

The physics of organic semiconductors has been extensively studied over the past two decades, with the aim of improving the performance of devices such as organic light-emitting diodes, solar cells, or field-effect transistors. Recently, increased attention has been placed on the role that electronic states that extend into the gap of the semiconductors play in charge-carrier transport, interface formation, and overall device performance [1–5]. Organic semiconductors are characterized by relatively small electronic couplings [6]; as a result, even a moderate energetic and structural disorder leads to the localization of all electronic states. This is in contrast to moderately disordered inorganic semiconductors such as amorphous silicon where only the states in the band tail are localized. The energy that separates the localized and extended states is referred to as the mobility edge. However, even in the case of disordered organic semiconductors it is useful to distinguish between states that effectively contribute to the charge transport (conducting states) and those located deep in the gap (trapping states) by introducing an effective transport level [7,8]. States that lie deeper in the gap than this effective transport level tend to hinder charge transport, leading to low effective carrier mobility. These trap states can originate from impurities and molecular defects in the semiconductor material [9–11]. In addition, dynamic and static disorder in the film and grain boundaries lead to fluctuations in polarization screening and, as a consequence, in the ionization energies and electron affinities throughout the layer, leading to tail-like states extending into the band gap [4,12].

Traps with similar energetic distributions have been a challenge for the development of amorphous silicon devices; in this material, hydrogenation is actively used to saturate dangling bonds and passivate the traps, greatly increasing the performance of devices [13]. Applying a related line of thought to organic semiconductors, it can be speculated that the filling of trap states should result in an improved performance of devices by increasing the effective carrier mobility. Theoretical considerations, as well as recent measurements at elevated doping levels, confirm that tail states of the matrix material can be filled by excess charge carriers and therefore no longer have a negative influence on the carrier mobility [1,2,14–16].

The addition of charge carriers via molecular or metal doping is a common technique to increase conductivity and decrease threshold voltages and injection barriers into transport layers of organic semiconductor devices [17]. Doping ratios used for devices and fundamental investigations usually range from 10^{-2} to 10^{-1} dopants per matrix molecule [18–24]. However, typical trap densities in disordered organic semiconductors are estimated to be in the range of 10^{17}–10^{19} cm^{-3} [8,11,25,26], corresponding to trap-to-molecule ratios of 10^{-4} to 10^{-2}. In order to probe the gradual filling of these states, investigations must be extended to ultralow doping levels.

For these studies, we use the prototypical electron-transport material C_{60} in combination with charge carriers released from the previously reported *n* dopant ruthenium(pentamethylcyclopentadienyl)(1,3,5-trimethylbenzene) dimer, $[RuCp^*(mes)]_2$ [27,28], shown in Fig. 1. We study the changes in Fermi-level position, conductivity, mobility, and activation energy for charge transport for molar doping ratios (MR) ranging from 2×10^{-4} to 3×10^{-1}, equivalent to dopant densities of 3.4×10^{17} to 3.7×10^{20} cm^{-3}. By extending this doping ratio to unprecedented low values, we establish clear trends in the evolution of transport parameters. Experimental results as well as kinetic Monte Carlo simulations confirm a distinct change in electronic behavior of the material when the doping concentration transitions from below typical trap densities, i.e., ultralow doping, to concentrations commonly used to enhance conductivity in organic devices.

The doping studies were conducted on C_{60} (Sigma Aldrich, 99.9% purity) and the *n* dopant $[RuCp^*(mes)]_2$, which was synthesized as previously reported [29].

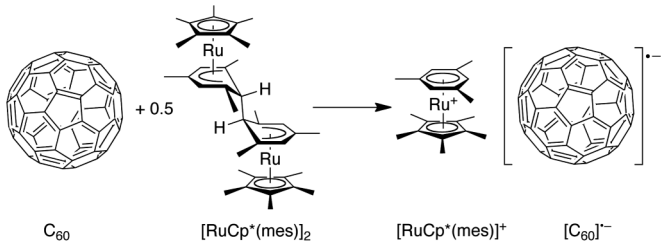

FIG. 1. Molecular structures of C_{60} and of the air stable *n*-dopant precursor $[RuCp^*(mes)]_2$. The dimer reacts with C_{60} to give two monomeric $[RuCp^*(mes)]^+$ cations and two fullerene radical anions.

The dopant dimer reacts with C_{60} to give two monomeric $[RuCp^*(mes)]^+$ cations and two fullerene radical anions in the evaporated layer; therefore, the MR throughout this Letter is given in reference to the number of monomeric cations. All films were prepared under ultrahigh vacuum (UHV) at base pressures below 5×10^{-10} Torr, by coevaporating matrix and dopant while the evaporation rates were independently controlled by quartz crystal monitors. Prior to deposition, C_{60} was degassed for at least 12 h to remove residual impurities from the source material.

The substrates prepared for UV photoemission (UPS) and inverse photoemission spectroscopy (IPES) measurements consisted of indium tin oxide (Thin Film Technology) covered by a 20 nm high-work-function poly(3,4-ethylenedioxythiophene):poly(styrenesulfonate) (PEDOT:PSS) (Sigma Aldrich) layer. A 5 nm buffer layer of intrinsic C_{60} was evaporated on PEDOT:PSS before depositing the *n*-doped layer in order to decouple the doped film from the substrate and prevent dopants from introducing an additional interface dipole. The thickness of the investigated doped layers was 20 nm. UPS was performed using the He(I) photon line (21.22 eV) from a He discharge lamp. The energy resolution of the measurement was 0.15 eV. A -5 V bias was applied to the sample to facilitate observation of the slow electron cutoff. IPES was performed in the same chamber, using a setup described elsewhere [30]. The energy resolution in IPES measurements was 0.45 eV.

The conductivity measurements were performed on quartz glass slides prepatterned with interdigitated gold electrodes (interelectrode gap of 150 μm), and the current through the layer was measured in the lateral direction. The thickness of the undoped C_{60} film was 100 nm, designed to provide a measurable current especially at low temperature, while the thickness of the more conducting doped layers was kept in the range of 15 to 30 nm. The C_{60} evaporation rate varied from 0.2 Å/s for the intrinsic and highly doped samples to 3 Å/s for the samples with lower doping levels. It was verified that the increased evaporation rate had no significant effect on the film conductivity or on the activation energy of the electron-transport process. Furthermore, neither film thickness nor evaporation rate had any significant impact on the film morphology, as measured via atomic force microscopy (AFM) [Figs. S1(a)–S1(c) in the Supplemental Material (SM) [31]]. The dopant evaporation rate varied from 0.02 Å/s to 0.0003 Å/s, respectively. The total thickness of the film was taken as the sum of matrix and dopant thicknesses, assuming equal densities for both; furthermore, the effective density of matrix molecules (1.4×10^{21} cm^{-3} for intrinsic C_{60} [32]) was modified for the doped layers by taking the addition of the dopants into account. Following room-temperature deposition, the samples were transferred under UHV to a temperature-controlled sample stage for variable-temperature (VT) current-voltage (*I-V*) measurements carried out with a Keithley 2400 SourceMeter. Before VT *I-V* measurements, the samples were vacuum annealed at 400 K for several hours. This step had been previously reported to remove some of the trap states present in the layer [33] and in the present work led to reproducible VT *I-V* curves in repeated temperature scans. Note that in the cases of moderate to high doping ratios, this initial annealing step has no effect on the film conductivity. Doping was found to be stable at these temperatures. The samples were then cooled down to 100 K at a rate of 1 K/ min and *I-V* measurements were recorded. The sample conductivity was determined at low electric fields from the Ohmic region of the current-voltage scans.

Kinetic Monte Carlo simulations were performed to analyze the data and gain information on trap density and distribution. Electron transfer was assumed to occur only between near neighbors in a cubic lattice model. The matrix material C_{60} was simulated as a cubic super cell with length $L = 50$ nm and $50 \times 50 \times 50$ lattice sites. Periodic boundary conditions were applied on all three directions. The electron transfer processes are described in the framework of the Miller-Abrahams model [34] (see SM [31] for details). For simplicity, all electrostatic interactions were ignored. A Gaussian distribution of density of states (DOS) was used for the conducting (band) states, and an exponential distribution for the band tail states. The model assumes a temperature-independent density of charge carriers distributed over the hopping (lattice) sites whereby the distribution of energy depth of the hopping sites determines the effective carrier mobility in the film [19,35]. In the simulations, the charge density is computed assuming that every dimeric dopant molecule introduces two charge carriers into the C_{60} matrix. The sites with exponential distribution of DOS were randomly selected before each simulation. Energies of all other sites were taken from the Gaussian distribution. All site energies were assigned before starting the simulations and were kept fixed during the simulations. Simulations were stopped once the effective conductivity ($\sigma = e\upsilon N_e/F$, where e is the elementary charge, N_e is the charge density, υ is the average velocity, and F is the applied electric field) converged to a constant value. The widths of the Gaussian (δ_G) and exponential (δ_E) distributions, the ratio of the total numbers of exponential to Gaussian states (N_E/N_G), and the attempt frequency (ν_0) that enter in the Miller-Abrahams model were obtained by fitting the experimental dependence of the conductivity on the molar

doping ratio at room temperature. The applied electric field is set in the calculations to 12 795 V/cm.

UPS and IPES measurements were performed on intrinsic C_{60} and doped layers to correlate changes in doping ratios with the movement of the Fermi level (E_F) within the gap of C_{60}. The resulting spectra can be found in Fig. S2 in the SM [31]. For the intrinsic C_{60} layer a work function (WF) of 4.83 eV is measured and the difference between E_F and the onset of the highest occupied molecular orbital (HOMO) edge is 1.57 eV, while the distance to the LUMO (lowest unoccupied molecular orbital) edge is 0.89 eV, leading to values of the ionization energy and electron affinity of 6.4 and 3.9 eV, respectively. With increasing doping concentration, the WF of the layer decreases as the Fermi level rises toward the LUMO. For a high doping ratio of 3.4×10^{-2}, the LUMO edge and E_F are separated by merely 50 meV. The changes in WF and HOMO position are plotted in Fig. 2 as a function of molar doping ratio. Note that, in view of the broadening of the HOMO feature at high doping ratios, which is noticeable in the top UPS spectrum of Fig. S2 in the SM [31], we plot the center of the peak for the HOMO position in Fig. 2 rather than the HOMO edge conventionally used to define the ionization energy. A clear break is observed in the slopes of both the WF and the HOMO peak position, at MR $\sim 6 \times 10^{-3}$. These data are consistent with the Fermi level starting from a position deep in the transport gap and, in the early stages of doping, moving rapidly through the relatively low density of deep trap states, giving large slopes for both the WF and the HOMO peak position versus MR. Once the traps are mostly filled, the variation in Fermi-level energy with doping slows down as E_F approaches the bottom of the C_{60} LUMO, and follows the 60 meV per decade of doping at room temperature expected from standard semiconductor theory; here, the relation between two different carrier concentrations $N_e^{(1)}$ and $N_e^{(2)}$ is a function of their respective Fermi-level positions $E_F^{(1)}$ and $E_F^{(2)}$ according to $N_e^{(1)}/N_e^{(2)} = \exp[(E_F^{(1)} - E_F^{(2)})/kT]$, where k is the Boltzmann constant and T the temperature.

To further investigate the changes observed between ultralow and moderate doping regimes, variable-temperature conductivity measurements were performed over a wide range of doping, varying in MR from 1.8×10^{-4} to 3.6×10^{-1} (see detailed temperature-dependent conductivity measurements data in Fig. S3 in the SM [31]). The observed changes in conductivity, mobility, and activation energy deduced from these data were analyzed using the kinetic Monte Carlo simulations. Figure 3(a) shows the dependence of the conductivity on MR at three different temperatures, 140, 296, and 400 K, both from

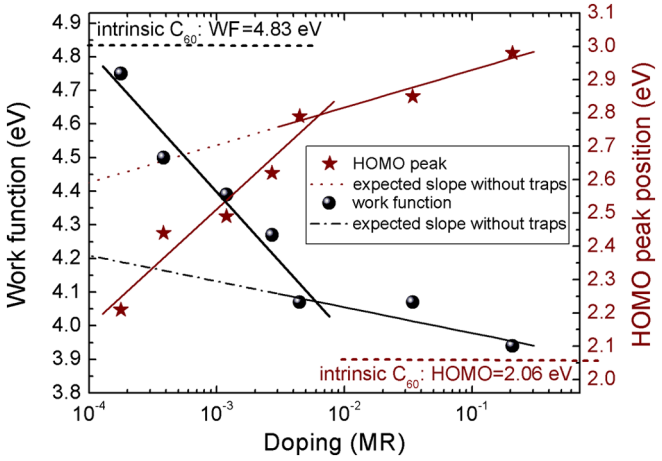

FIG. 2 (color online). Change in work function and HOMO peak position with respect to the Fermi level upon doping, deduced from the UPS spectra given in Fig. S2 in the SM [31]. Because of the broadening of the HOMO feature at high doping, the HOMO position is given by the peak value. The corresponding values for the intrinsic C_{60} film are given by the top and bottom dashed horizontal lines, respectively.

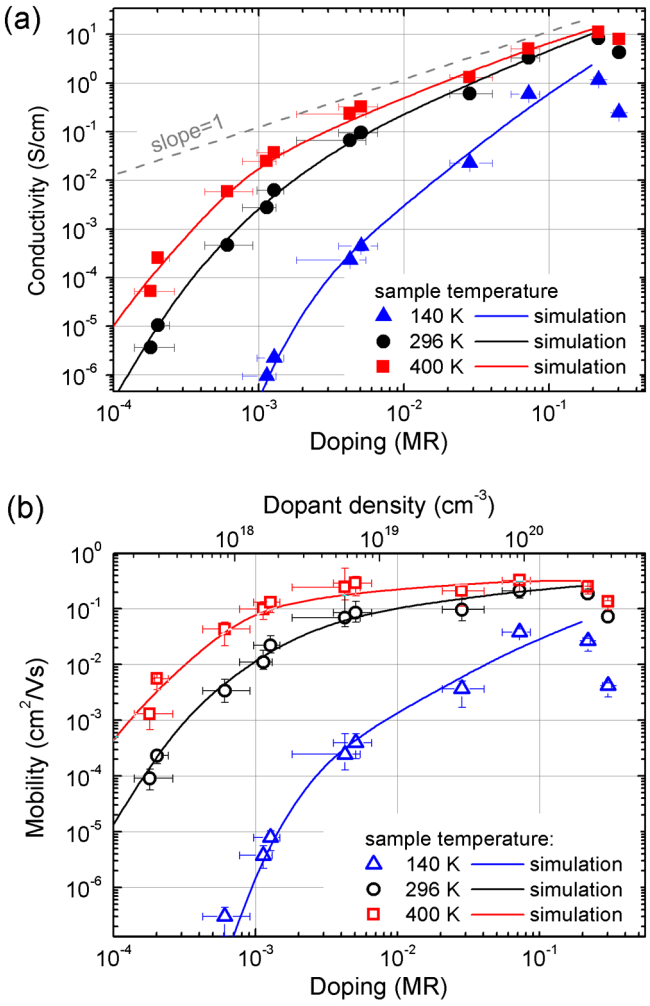

FIG. 3 (color online). (a) Experimental data (symbols) and simulation results (lines) for the conductivity of a C_{60} layer as a function of doping with $[RuCp^*(mes)]_2$ for three different temperatures; a line with a slope of unity is given as guide for the eye. (b) Experimental data (symbols) and simulation results (lines) for the change in C_{60} mobility upon trap filling deduced from the conductivity data shown in (a) using $\mu_e = \sigma/eN_e$.

experiments (symbol) and simulations (line). An excellent fit is obtained between the computed values of σ and the experimental data set at 296 K when assuming $\delta_G = 64$ meV, $\delta_E = 128$ meV, $N_E/N_G = 0.007$ and $\nu_0 = 7 \times 10^{12}$ s^{-1}. All these parameters are subsequently kept constant for the 140 and 400 K calculations. Therefore, the excellent agreement between theoretical and experimental data obtained for all temperatures suggests that the model describes reasonably well the actual density of states in the present system. In agreement with the UPS and IPES results, a clear break in the slope is also observed in this log-log plot around MR $\sim$ (2–4) $\times 10^{-3}$. For the room-temperature and high-temperature measurements, the conductivity increases almost linearly with MR in the moderate-to-high doping regime, and superlinearly in the low doping regime. These results indicate that electron transport in the undoped material is dominated by carrier trapping, and that trap filling by carriers released by the dopants leads to an increase in mobility. The change in slope occurs at the level of doping at which most of the traps are filled, with the unity slope [dashed line in Fig. 3(a)] reflecting the transport of an increasing density of mobile carriers. The unity slope is not observed in the low temperature data set, since trapping continues to play an important role even at high doping ratio. These conclusions are also supported by the results of the Monte Carlo simulations. Indeed, the change in slope occurs when all the states below the point where the Gaussian and exponential distributions cross become filled (see Fig. S4 in the SM [31]). This point is located about 0.23 eV below the maximum of the Gaussian density of states, and the total number of states below this energy level is about 1.9×10^{18} cm^{-3}. For the highest doping ratio of MR = 0.3, a decrease in conductivity is observed, since the large number of dopants leads to a severe disruption of the morphology of, and/or molecular order in, the film [see AFM image Fig. S1(d) in the SM [31]], and, presumably, to the introduction of new trap states. This behavior is not captured by the hopping model, which leads to a discrepancy between the experimental data and simulation results. At room temperature, the highest conductivity is 8.28 S/cm for MR = 0.22.

Based on the derived values for σ, we can also calculate the lower limit of the change in effective electron mobility ($\mu_e = \sigma/eN_e$) upon doping. The resulting experimental data (symbols) as well as the simulation results (lines) are shown in Fig. 3(b). Here, the effect of trap filling on transport becomes most obvious. In the room-temperature measurement, the lowest doping ratio of 1.8×10^{-4} yields a mobility of 9.1×10^{-5} cm^2/(V s), which compares well with a previously published value of 4×10^{-5} cm^2/(V s) for undoped C_{60} [36]. Increasing the dopant density by 1 order of magnitude results in a rapid rise of the mobility by nearly 3 orders of magnitude due to the filling of the trap states. Beyond MR $\sim 5 \times 10^{-3}$, the rise in mobility slows down considerably, with an increase of only a factor of 5 for a 2 orders of magnitude increase in dopant concentration. The rapid increase in mobility at very low doping ratios and the nearly constant mobility value for moderate or high doping is in agreement with previous observations [5,37]. The highest room-temperature mobility is 0.21 cm^2/(V s), achieved for MR = 7.2×10^{-2}.

The analysis of the change in conductivity with temperature provides insight into the dopant-induced change in activation energy of the hopping process, E_{act}:

$$\sigma = \sigma_0 e^{-E_{\text{act}}/kT}, \quad (1)$$

where σ_0 is a preexponential factor; E_{act} and σ_0 values obtained for the different doping levels can be found in Table S1 in the SM [31]. The experimental data (symbols) and simulation results (lines) are illustrated in Fig. 4 in a semilogarithmic plot of E_{act} versus MR. Again, good agreement between experimental data and simulation results can be demonstrated using the fitting parameters obtained from the conductivity data. As expected from the previous observations, a strong decrease in E_{act} is observed with doping, indicating reduced trapping of charge carriers brought about by trap filling and the shift of the Fermi energy closer to the transport level with concomitant increase in carrier density. At very low MR, the activation energy shows the strongest dependence on doping, and a decrease in slope is again found around MR = (2–4) $\times 10^{-3}$. The lowest observed E_{act} is 39 meV at MR = 7.2×10^{-2}, which is smaller than previously reported values for C_{60} doped with acridine orange base (150 meV [23]), or with $Cr_2(hpp)_4$ (50 meV [24]). Since the addition of dopants not only provides more charge carriers that can fill trap states, but at the same time introduces new traps due to Coulomb interaction [38] and disruption of the packing of the acceptor molecules, it can be expected that different dopants lead to different changes in activation energy. The observation of the very

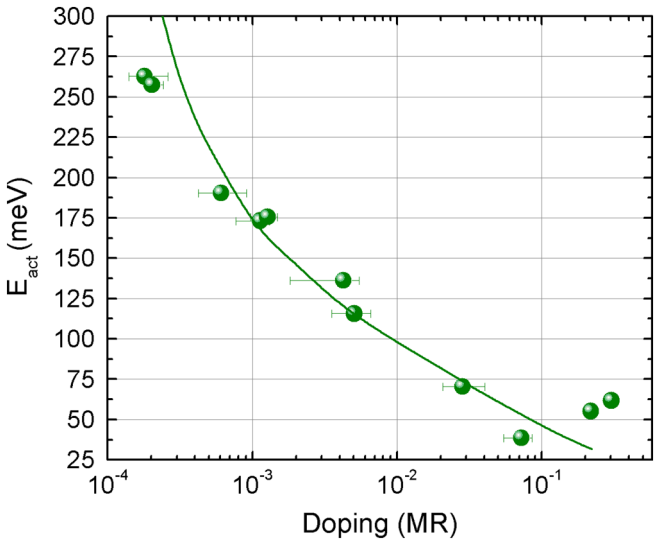

FIG. 4 (color online). Activation energy versus molar doping ratio obtained from the slope of the variable-temperature conductivity measurements (symbols) and Monte Carlo simulations (line).

low activation energy achievable with $[RuCp^*(mes)]_2$ suggests that few additional deep traps are formed, at least at low-to-moderate doping ratios.

To conclude, we were able to unambiguously pinpoint both experimentally and theoretically the transition between trap state filling and the more conventional doping regime in the organic semiconductor C_{60}, using ultralow n-doping levels in combination with kinetic Monte Carlo simulations. The best fit between data and simulation predicts an exponential distribution of trap states with a total density of 1.9×10^{18} cm^{-3}; this coincides well with reported trap densities in C_{60} of 10^{18}–10^{19} cm^{-3} [8]. The transition has a significant impact on the rate of change of film conductivity, mobility, activation energy, and position of the Fermi level versus doping concentration. Below this transition point, which occurs here at a molar ratio of (2–6) $\times 10^{-3}$, the charge-transport properties and Fermi-level position are dominated by trap states. Once all the traps are filled by dopant-induced charge carriers, the C_{60} mobility nearly saturates around 0.1 to 0.2 cm^2/(V s) at room temperature, and the changes in conductivity and Fermi-level position follow standard semiconductor theory. Controlled ultralow doping appears therefore to be an effective way to passivate unwanted traps in an organic semiconductor film, thereby opening avenues to further improvements of organic devices, in particular, solar cells where charge-carrier densities are on the order of typical trap densities.

This work was supported by Solvay S. A., the Office of Naval Research (N00014-11-1-0313), and the National Science Foundation (DMR-1005892). S. O. acknowledges support from the German Academic Exchange Service (DAAD). Fruitful discussions with Professor Sigurd Wagner are gratefully acknowledged.

*solthof@princeton.edu
†kahn@princeton.edu

[1] F. Deschler, E. Da Como, T. Limmer, R. Tautz, T. Godde, M. Bayer, E. von Hauff, S. Yilmaz, S. Allard, U. Scherf, and J. Feldmann, Phys. Rev. Lett. **107**, 127402 (2011).
[2] M. M. Mandoc, F. B. Kooistra, J. C. Hummelen, B. de Boer, and P. W. M. Blom, Appl. Phys. Lett. **91**, 263505 (2007).
[3] S. Scheinert, K. P. Pernstich, B. Batlogg, and G. Paasch, J. Appl. Phys. **102**, 104503 (2007).
[4] J. Rivnay, R. Noriega, J. E. Northrup, R. J. Kline, M. F. Toney, and A. Salleo, Phys. Rev. B **83**, 121306 (2011).
[5] Y. Zhang, B. de Boer, and P. W. M. Blom, Phys. Rev. B **81**, 085201 (2010).
[6] V. Coropceanu, J. Cornil, D. A. da Silva Filho, Y. Olivier, R. Silbey, and J.-L. Brédas, Chem. Rev. **107**, 926 (2007).
[7] V. I. Arkhipov, E. V. Emelianova, and G. J. Adriaenssens, Phys. Rev. B **64**, 125125 (2001).
[8] W. L. Kalb, S. Haas, C. Krellner, T. Mathis, and B. Batlogg, Phys. Rev. B **81**, 155315 (2010).
[9] W. L. Kalb, K. Mattenberger, and B. Batlogg, Phys. Rev. B **78**, 035334 (2008).
[10] C. Krellner, S. Haas, C. Goldmann, K. P. Pernstich, D. J. Gundlach, and B. Batlogg, Phys. Rev. B **75**, 245115 (2007).
[11] H. T. Nicolai, M. Kuik, G. A. H. Wetzelaer, B. de Boer, C. Campbell, C. Risko, J.-L. Brédas, and P. W. M. Blom, Nature Mater. **11**, 882 (2012)
[12] D. V. Lang, X. Chi, T. Siegrist, A. M. Sergent, and A. P. Ramirez, Phys. Rev. Lett. **93**, 086802 (2004).
[13] D. S. Brotherton, Semicond. Sci. Technol. **10**, 721 (1995).
[14] V. I. Arkhipov, P. Heremans, E. V. Emelianova, G. J. Adriaenssens, and H. Bassler, J. Non-Cryst. Solids **338**, 603 (2004).
[15] C.-T. Lee and H.-C. Chen, Org. Electron. **12**, 1852 (2011).
[16] Y. Zhang, B. de Boer, and P. W. M. Blom, Adv. Funct. Mater. **19**, 1901 (2009).
[17] K. Walzer, B. Maennig, M. Pfeiffer, and K. Leo, Chem. Rev. **107**, 1233 (2007).
[18] M. Pfeiffer, A. Beyer, T. Fritz, and K. Leo, Appl. Phys. Lett. **73**, 3202 (1998).
[19] R. Schmechel, J. Appl. Phys. **93**, 4653 (2003).
[20] R. C. Haddon, A. F. Hebard, M. J. Rosseinsky, D. W. Murphy, S. J. Dulcos, K. B. Lyons, B. Miller, J. M. Rosmilia, R. M. Fleming, A. R. Kortan, S. H. Glarum, A. V. Makhija, A. J. Muller, R. H. Eick, S. M. Zahurak, R. Tycko, G. Dabbagh, and F. A.Thiel, Nature (London) **350**, 320 (1991).
[21] C. K. Chan, W. Zhao, S. Barlow, S. Marder, and A. Kahn, Org. Electron. **9**, 575 (2008).
[22] S. Olthof, W. Tress, R. Meerheim, B. Luessem, and K. Leo, J. Appl. Phys. **106**, 103711 (2009).
[23] F. Li, M. Pfeiffer, A. Werner, K. Harada, K. Leo, N. Hayashi, K. Seki, X. Liu, and X.-D. Dang, J. Appl. Phys. **100**, 023716 (2006).
[24] T. Menke, D. Ray, J. Meiss, K. Leo, and M. Riede, Appl. Phys. Lett. **100**, 093304 (2012).
[25] J. Schafferhans, A. Baumann, A. Wagenpfahl, C. Deibel, and V. Dyakonov, Org. Electron. **11**, 1693 (2010).
[26] S. Yogev, E. Halpern, R. Matsubara, M. Nakamura, and Y. Rosenwaks, Phys. Rev. B **84**, 165124 (2011).
[27] S. Guo, S. B. Kim, S. K. Mohapatra, Y. Qi, T. Sajoto, A. Kahn, S. R. Marder, and S. Barlow, Adv. Mater. **24**, 699 (2012).
[28] Y. Qi, S. K. Mohapatra, S. B. Kim, S. Barlow, S. R. Marder, and A. Kahn, Appl. Phys. Lett. **100**, 083305 (2012).
[29] O. V. Gusev, M. A. Ievlev, M. G. Peterleitner, S. M. Peregudova, L. I. Denisovich, P. V. Petrovskii, and N. A. Ustynyuk, J. Organomet. Chem. **534**, 57 (1997).
[30] C. I. Wu, Y. Hirose, H. Sirringhaus, and A. Kahn, Chem. Phys. Lett. **272**, 43 (1997).
[31] See Supplemental Material at http://link.aps.org/supplemental/10.1103/PhysRevLett.109.176601 for additional experimental data and Monte Carlo simulation details.
[32] N. Hayashi, H. Ishii, Y. Ouchi, and K. Seki, J. Appl. Phys. **92**, 3784 (2002).
[33] B. Mishori, E. A. Katz, D. Faiman, and Y. Shapira, Solid State Commun. **102**, 489 (1997).
[34] A. Miller and A. Elihu, Phys. Rev. **120**, 745 (1960).
[35] I. I. Fishchuk, V. I. Arkhipov, A. Kadashchuk, P. Heremans, and H. Bassler, Phys. Rev. B **76**, 045210 (2007).
[36] K. Hoshimono, S. Fujimori, S. Fujita, and S. Fujita, Jpn. J. Appl. Phys. **32**, L1070 (1993).
[37] B. Maennig, M. Pfeiffer, A. Nollau, X. Zhou, K. Leo, and P. Simon, Phys. Rev. B **64**, 195208 (2001).
[38] V. I. Arkhipov, P. Heremans, E. V. Emelianova, and H. Bassler, Phys. Rev. B **71**, 045214 (2005).